February 13, 2009; CEA Saclay
Internal report: IRFU-09-15
EURISOL DS/Task#5
www.eurisol.org

Radiation protection aspects of the EURISOL Multi-MW target shielding

D. Ene, J.-C. David, D. Doré, B. Rapp, D. Ridikas

IRFU/SPhN, CEA Saclay, 91191 Gif-sur-Yvette, France

Abstract

An ambitious European project EURISOL DS (FP7) deals with the design of new generation RIB production facility based on ISOL method. The future factory is characterized by a 4 mA proton beam of 1 GeV (4 MW power) impinging on a liquid Hg target-converter, which in turn is surrounded by a number of small actinide fission targets, each aiming at ~10^{15} fissions/s. In this context, Monte Carlo simulations using MCNPX version 2.5.0 were performed to optimize the bulk shielding of this EURISOL Multi-MW target. Using the obtained neutron flux and energy spectra, activation calculations with DCHAIN-SP2001 code were carried out to create an activation map of the entire shielding structures. Some quantitative comparisons between DCHAIN-SP2001 and CINDER'90 material evolution codes were also performed. Two approaches of the shielding activation zoning were assumed for the radioactive wastes study: i) the activity estimates were done at the level of a fine annular mesh grid with radius and height of 10 cm (FM approach) and ii) thick layers of 100 cm thickness (TL approach) were used to derive the total activity. Finally, the classification of the radioactive wastes based on IAEA clearance levels was further elaborated for seven decay time periods after target operation shutdown. Comparison of the results obtained for the two approximations used is discussed. Using the same procedure, an estimation of the produced radioactivity inside the soil surrounding the shield (to be used as source term for the contaminant transport) was further derived.

Estimates of the air activation in the shielding gap were also determined and the obtained results are compared and discussed. The results of this study will contribute to the estimates of the overall timescale and costs of the EURISOL facility having also a strong impact on the decision and strategy to be adopted for the facility dismantling, waste classifications, and their final disposal.

1. Introduction.

Worldwide the study of exotic nuclei is in rapid advance. Major projects are planned or already underway in Europe, the USA and Japan to design and build the next generation radioactive ion beam (RIB) production facilities. EURISOL [1] is the European common effort in designing and planning a next generation RIB factory able to deliver secondary beams of the order of 10^{13} pps at energies up to 150 MeV u^{-1}. The proposed schematic layout of the facility contains: a high-energy high-intensity proton driver accelerator, several target ion-source systems, a mass-separator and a post-accelerator. The EURISOL facility will deliver the secondary beams of unprecedented intensities thanks to the new generation single-stage ISOL targets (three direct targets of 100 kW of beam power are foreseen) together with a multi-MW two-stage target assembly. In the multi-MW target high intensity RIBs of neutron rich isotopes are produced by fission in actinide targets placed in the secondary neutron flux produced in the liquid mercury spallation target.

The increase of the RIB intensities by a factor of 100-1000 compared to presently operating facilities will give rise to challenging issues in terms of nuclear safety and radioprotection. In the framework of the radiation characterization and safety studies within the EURISOL DS/Task 5 detailed calculations were performed to estimate the prompt and residual radiation fields in the multi-MW target and its surroundings. An important safety and radioprotection objective is to demonstrate the feasibility of the EURISOL project over the entire life cycle, including decommissioning. The large quantities of radioactive wastes produced in the bulk shielding of the MMW target at the end of the EURISOL facility operational lifetime require radiological characterization. In this context it is important to assess the issues related to radioactive wastes arising during the facility operation.

This work is focused on the approach used to assess the radiological characterisation and to support waste analysis for the multi-MW power target shielding being the most challenging both in terms of technological and safety issues. Identification of the key radio-nuclides that are representative for the activation of a certain shielding materials as well the estimation of the specific activity per radionuclide are very important criteria to decide the dismantling strategy for the entire facility. The choice of the method to be used for the treatment of the radioactive wastes and their classification in the view of the final disposal is an essential point of the radiological safety in the shielding design. The safe handling of radioactive waste is recognised as vital to ensure protection of human health and the environment. Therefore, careful consideration of these important aspects has to be given since the very early stage of the design of the facility because they contribute essentially to the entire cost estimates and are important for the overall project planning and timescales.

The major objective of the present paper has been to characterize and assess the EURISOL multi-MW power target surroundings in terms of the nuclear safety functions that have to be provided by the design in order to meet the requirements concerning the protection of the workers, public and the environment.

Additionally in order to apply the ALARA principle, through the development of the method used to support this study an important concern was the choice of the appropriate tools and procedures able to derive accurately required estimates. From this reason more than one computer code and/or approach were comparatively analysed.

The next chapter will give an overview of the different aspects that are relevant for modelling and simulation methods applied in the study. In chapter 3 we describe the results of the calculations. The outcomes of this work are presented first for prompt radiation simulations, then for the activation. This section concludes with the waste classifications. Soil and groundwater radioactivity estimates are also reported. Air activation resulted in the shielding gap is further studied and the results are analyzed.

2. Calculation procedure.

The starting point for the present analysis is the study of the Ref. [2], where a preliminary reduced shielding model of the target was investigated by means of the FLUKA Monte Carlo code [3]. This basic shielding configuration was further predicted based on the extrapolation of the obtained results to meet the dose rate criterion of 1 $\mu Sv\ h^{-1}$.

This shielding concept is used here and developed by means of the MCNPX version 2.5.0 code [8] to provide a complete characterisation as far as the radioprotection is concerned. Dose rates, energy deposition and fluxes were estimated for a considerably more extended shielding configuration as well as neutron energy spectra and corresponding activation in the appropriate locations within the plane cutting horizontally and vertically through the centre of the target. A complete map of the radioactivity was further deduced by calculation of the activity of each shielding zone using the scaling of the total flux ratio. A clearance factor was determined for each material from the obtained specific activity and clearance limit defined in [5-6]. The allocation of each component to a waste category and further summation of activities and masses by material type inside its class followed. For each material, the activity, mass and volume in each of the three waste categories recommended in [4] are given at periods of 0.27 (100 days), 3, 10, 25, 100, 300 and 1000 years from the target operational shut down. Soil and groundwater radioactivity estimates are also derived using the same calculation procedure. Air activation, obtained in the shielding gap, was further studied using two different methodologies and the results are compared and analyzed.

2.1 Prompt radiation simulations.

2.1.1 Geometry model.

The target model (Fig. 1 left panel) consists of a spallation neutron source based on the liquid mercury target (50 cm long, 16 cm diameter) converting the incident proton beam into neutrons. The target is surrounded by two ring-shaped tantalum containers filled with actinide carbide (UCx or ThCx) where, through neutron induced fissions reactions, the fission products are produced. A graphite moderator encloses both the spallation convertor and fission targets. The whole target assembly is placed in a stainless steel vacuum chamber (100 cm long, 100 cm diameter). Detailed description of this multi-MW target assembly is given in [7]. Because extraction of the radioactive isotopes as well as the handling of the target items are conceived to be done on axial direction, a bulk radiation shielding might be an appropriate design option for this target configuration. For this reason the target shielding was modelled as a massive cylinder block placed at 60 cm from the beam axis and at 20 cm distance from both axial ends of the void chamber. It was a design requirement to minimize the volume inside the shielding around the target system in order to facilitate the evacuation of the target area and minimize the volume of activated air.

In the shielding model (see Fig. 1) the concrete shield is extended to a depth of 900 cm beyond the one metre stainless steel (SS) shield layer both in the radial and axial directions. In addition, in this geometry configuration one metre thick layer of soil surrounds the concrete. The geometrical centre of the target ensemble is placed at 30 cm from the beam-target interaction point. The proton beam strikes the target in the middle plane coming from the right (negative direction of the OZ axis). To facilitate the calculations, a cylindrical grid was used to divide the shielding into axial and radial zones of 100 cm thickness. The cutting planes delimiting these zones are shown in the same Fig.1 (right panel). In the forward direction with respect to the proton beam axis the geometry model contains small cylindrical cells (radius of 10 cm, height of 10 cm) set on each plane separating the axial shielding zones. Annular cells of 10 cm thick placed outwards at the inner edge of each radial shielding zone were represented in the central plan perpendicularly to the proton beam direction. These locations considered representative for the bulk layers inside the shielding were incorporated in the model to estimate detailed energy distributions of the flux needed for activation calculations.

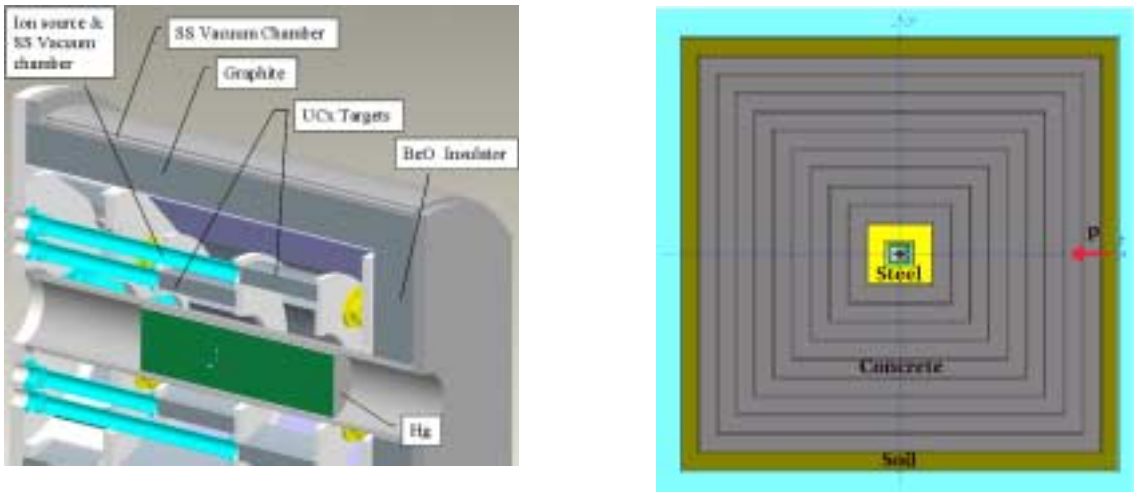

Figure 1: Calculation model used in simulations: details of the Multi MW target (left) and associated shielding concept (right). Also see text for details.

2.1.2 Simulation technique.

Simulation of the complex nuclear processes in the target and its surroundings was done using MCNPX2.5.0. The physics options for the particle-nucleus interaction and subsequent transport calculations were chosen following the conclusions of the code benchmarks done in [9]. INCL4 intra-nuclear cascade coupled with ABLA evaporation models were used to determine neutron production in the problem, while ISABEL-RAL combination was selected to correctly predict the tritium production at high energy [9].

In the simulations the 4 MW, 1 GeV proton beam was modelled with a Gaussian profile (1σ = 1.5 cm). All particles were transported with an energy threshold of 1 keV except the neutrons (down to thermal energies).

To determine the quantities of interest, the mesh-based weight window generator within the MCNPX code was employed as variance reduction technique inside the shielding walls. This technique produces an optimal importance function inside every cell defined initially by a virtual cylindrical grid covering the geometry. A preliminary investigation has shown the superiority of weight window generator technique versus the exponential transform biasing method used to calculate the neutron flux. It was found that the results obtained by means the exponential transform technique might be unreliable in the fast energy component of the neutron spectrum (energies higher than 200 keV), where underestimation of the analogue results reaches a factor of 3. On the other hand, the weight window method results are rather stable compared to the non-variance calculations. Nine iterative simulations, each transporting $2*10^6$ primary protons were used to calculate detailed energy neutron flux distributions at the representative locations detailed in the previous subsection.

A refined mesh (with a step of 10 cm) overlapping the whole shielding geometry on a cylindrical grid was also used to display the particle fluxes, associated dose rates and energy deposition. The options for the dose conversion coefficients (DCF) used to fold the particle track-length spectra were as follows: i) ICRP-74 1996 ambient DCF for neutrons and ii) ANSI/ANS 6.1-1991 for photons. The nuclear data library underlying all present simulations was based mainly on the ENDF/B VII evaluated file.

2.2 Activation of shielding structures.

Activation calculations were performed both by means of CINDER'90 [10] and DCHAIN-SP

2001 [11] computer codes. Both codes are based mainly on EAF4.1 library [12] and are able to calculate, in conjunction with a Monte Carlo particle transport code, the residual nuclide production including fission products over the whole energy range of interest. To this end the two distinct parts obtained from MCNPX code: i) low energy (E < 20 MeV) neutron flux distributions and ii) high energy reaction product (E > 20 MeV) estimates in the physics model region are used as input in the activation codes and combined to solve the modified Bateman equations. Spallation products derived from MCNPX by means of HTAPE module [8] are read directly in CINDER'90 code and via a format translation utility in DCHAIN-SP.

The results of the two codes were analysed comparatively. It was found that both codes provide similar results. This confrontation of the codes is of interest to assess and validate the present approach for radionuclide inventory and specific activity estimates. However, because DCHAIN-SP systematically gives activation results somewhat higher than those obtained by CINDER'90 it was decided that they will be used (being conservative) in this study. Therefore later in the text these results are reported without any further specification.

Compositional data, nuclide content and impurity elements present within activated materials have been chosen as follows:

i) AISI304LN SS composition (ρ = 7.92 g cm^{-3}) taken from [13] with the chemical composition (weight fractions): Fe 70.6 %, Cr 18 %, Ni 10 %, Si 0.1 %, and C, ^{59}Co, V, ^{55}Mn, S, P each less than 0.1 % ;

ii) ordinary concrete (ρ = 2.3 g cm^{-3}) chemical composition of the research reactor ULYSSE (CEA Saclay) [14]: O 52.9 %, Si 21.8 %, Ca 17.4 %, C 3.7 %, Al 1.5 %, Fe 1 %, K 0.5 %, H 0.4 %, Na 0.4 %, Mg 0.3 %, S 0.1 % and other more than 70 impurities up to Uranium;

iii) soil composition (ρ = 1.6 g cm^{-3}) : O 50.1 %, Si 37.3 %, Ti 9.7 %, Fe 1.5 %, K 0.9 %, Al 0.4 %, Zn, Pb, Mn, P, Cr, Ni, Cu each less than 0.1 % as well as groundwater composition containing some traces of S, Cl, P, Na, Ca, Mg, Fe, Al to Hg were derived from several soil-samples from Krauthausen location (North Rhine-Westphalia, Germany) see [15];

iv) air composition (ρ = 0.001205 g cm^{-3}): N 75.56 %, O 23.16 %, Ar 1.28 %

The irradiation history was conservatively simulated by considering 40 years of continuously operation at 2.28 MW (what correspond to 7 months of full power irradiation per year) followed by variable decay times up to 1000 years after the facility shut-down.

Separate activation calculations were performed for each representative location and specific material identified to be present within the planes cutting horizontally and vertically through the centre of the target. The activities between the cutting planes were scaled from the results for the nearest entrance central location using the ratios of the total flux in the associated zones. Such an approximation is valid when the activation product is produced by a single step reaction. This requirement is satisfied by most of the dominant activation products.

Depending on the degree of the precision two activation zoning approximations were analysed: i) an accurate zoning assuming the fine mesh activity estimates inside cylindrical mesh tally cells described in chapter 2.1.2, (Fine Mesh - FM approach), and ii) a conservative one where the activity was derived inside thick layers of 100 cm thickness, (Thick Layer - TL approach).

2.3 Waste management: methodology for classification to non-active material (clearance).

Because the EURISOL facility site is not yet identified and thus the regulations of a specific host country can not be applied, it was decided to use in this study the waste management methodology recommended by the IAEA. This approach is based on the concept of clearance. Clearance is defined as the removal of the radioactive materials or radioactive objects within the authorised practices from any further regulatory control by the regulatory body. The classification system proposed by the IAEA [4] places the radioactive waste into one of following three classes:

1. HLW: High Level Wastes

Highly radioactive liquid

Heat generating waste (> 2 kW m^{-3})

2. LILW: Low and Intermediate Level Wastes divided in:

2.1 LILW-LL: Low and Intermediate Level Wastes -Long Lived

Half life > 30 years

Long lived alpha emitters: > 400 Bq g^{-1} average

> 4000 Bq g^{-1} individual package

2.2 LILW-SL: Low and Intermediate Level Wastes -Short Lived

Half life < 30 years

3. EW: Exempted Wastes

Wastes below clearance levels giving < 0.01 mSv y^{-1} to a member of the public.

References [5-6] give clearance levels values (L_i) for a number of nuclides and a general formula that can be used to calculate the level for any other nuclide. This formula is given in Eq. 2.1:

$$L_i = \min\left\{\frac{1000}{E_\gamma{}^i + 0.1 * E_\beta{}^i}, \frac{D_w}{e_{inh}{}^i}, \frac{D_w}{100 * e_{ing}{}^i}\right\}, \tag{2.1}$$

where D_w = 20 mSv y^{-1}, i.e. the dose limit for radiation workers [16] and for the i_{th} nuclide:

$E_\gamma{}^i$ - effective photon emission energy (MeV);

$E_\beta{}^i$ - effective beta decay emission energy (MeV);

e_{inh} - committed effective dose equivalent from inhalation (Sv Bq^{-1});

e_{ing} - committed effective dose equivalent from ingestion (Sv Bq^{-1}).

Eq. 2.1 is used to calculate L_i values for all nuclides not given explicitly in references [5-6]. The recommended clearance levels [5-6] range from about 0.1 Bq g^{-1} (^{60}Co and most of impurities presenting materials), 100 Bq g^{-1} for ^{3}H, 1000 Bq g^{-1} for ^{55}Fe to about 10^4 Bq g^{-1} for ^{59}Ni. These values were derived through many dedicated studies and are based on the limiting annual dose of 0.01 mSv to members of public.

The clearance index (CI) for a material containing a mixture of radio-nuclides is calculated by Eq. 2.2, where A_i is the specific activity due to the component nuclide i and L_i is the clearance level for the nuclide i, namely

$$CI = \sum_{i}^{Nnuclides} \frac{A_i}{L_i}. \tag{2.2}$$

In Eq. 2.2 activities and clearance levels have units of Bq g^{-1}.

From the analysis of the resulted decay heat production in the shield it was found that no waste would fall into the IAEA HLW category. Thus, consistent with the IAEA classification system the allocation to a waste category for each decay period considered was done in this study as follows:

i) The materials were classified as **LILW-LL** if CI for nuclides with half lives more than 30 years was greater than 1;

ii) If this was not the case but CI for all nuclides (those with half lives more than 30 years plus those with half lives less than 30 years) was greater than 1 the materials were classified as **LILW-SL**;

iii) Any material for which CI was less than or equal to 1 were classified as **EW**.

The clearance levels data used in the present evaluations were taken from the ANITA-2000 code [17]. Clearance Data library (FL1 file) were made available thanks to D. Cepraga [18]. Note that the ANITA library contains the set of clearance data defined in IAEA-TECDOC-855 [5] together with

calculated values derived using Eq. 2.1, where E_γ^i and E_β^i are taken from FENDL D-2.0 library and the hazard data are obtained from the International Commission on Radiological Protection Publication of dose coefficients ICRP-72 [19]. Furthermore this database was updated here with the revised L_i values given in [6], i.e. they are more stringent than the previously issued values recommended by the IAEA. For instance, the 2004 guidelines suggest lower clearance levels for ^{3}H (by a factor of 30), for ^{60}Co and $^{59,63}Ni$ (by a factor of 3) compared to the previous 1996 standards. That implies consequently that for these materials longer time will be needed to reach clearance.

Based on the methodology described above, the DCHAIN-SP2001 code was adapted to read clearance levels library and to calculate the CI for each material at each decay time. In addition, to facilitate the classification into a waste category the resulted CI were sorted out by the lifetime value of 30 years of the constituent nuclides in the material.

2.4 Source term for contaminant transport

The production of radioactive nuclides in the surrounding soil was determined using the same calculation procedure as for the shielding structures. The groundwater activation was estimated based on the rough assumption that the ground water table replaces the soil layer around the concrete shielding (see Fig.1).

2.5 Air activation

For low-density materials (for instance the gases) the calculation of isotope production using the physics models by means of Monte Carlo method does not give reliable results due to very low interaction probability. The method commonly used to estimate the induced radioactivity in the air consists in the folding of particle track-length spectra with evaluated isotope production cross sections. Thus in an air region the yield Y_i of the radionuclide i is obtained from the Eq.2.3

$$Y_i = \sum_{j,k} N_j \int \sigma_{ijk}(E)\Phi_k(E)dE \,. \tag{2.3}$$

where:

N_j = the atomic concentration per cm^3 of element j in the material;

σ_{ijk} = the cross section for the production of the radionuclide i in the reaction of a particle of type k and energy E with a nucleus of the element j;

Φ_k = track-length spectrum of the particles of type k and energy E.

This approach was used here for the determination of the activation of the present between the target vacuum chamber and the shielding (volume=$7.446*10^5$ cm^3).

As first approximation in Eq.2.3 the track-length spectra from the MCNPX simulations were post-processed together with the available interaction cross sections of radionuclide production from the air constituents (Cross Section - CS approach), data extracted from the EXFOR database and ENDF/B-VI [20]. In addition, a more accurate estimation of the nuclide yields was done using the option implemented in the PHITS code [21] that changes the original Monte Carlo sampling to allow the folding on-line of the particle track-length spectra with evaluated isotope production cross sections (PHITS approach). PHITS code uses the combination of the Bertini intranuclear cascade model [8] and the generalized evaporation model [22] to better estimate the nucleon induced light target interaction cross sections. Detailed analysis of the predicted excitation functions of the nuclides produced from the reaction on nitrogen and oxygen targets irradiated by nucleons [23] shows that for proton induced reactions in the energy range beyond 10 MeV the accuracy of the nuclide yields is still in the level of a factor 2 to 3. A simplified geometry model that takes into consideration only 50 cm from SS shield around the air cavity was used in PHITS simulations.

Both radionuclide yields obtained from the two methods described above were further used as

input in the two activation codes together with the low energy neutron flux distributions (see chapter 2.2) for a comparatively analysis of the time evolution of the radioactive nuclides produced in the air region. A conservative scenario of 3000 hours of continuous irradiation was assumed in the calculations. From the comparison of the code results, conversely with the previous conclusion it was found that CINDER'90 results give higher activation levels compared to DCHAIN, and therefore due to the conservative criterion, are presented in this paper.

3. Results and discussion.

The results presented are normalized to 1 mA intensity proton beam on the target to allow easily the desired scaling to other values. Only in case of the dose rates estimates needed for sizing of the shield, the discussion refers to the full proton beam intensity (4 mA).

3.1 Prompt radiation transport

3.1.1 Dose rates and energy deposition.

Neutron dose rates in the forward direction resulted from the simulations are shown in Fig.2. The concrete thicknesses required to meet the design constraint were derived based on both forward and laterally H*(10) obtained results. It was found through the analysis of neutron attenuation curve profiles in the concrete that the concrete shield has to be extended to a depth of 900 cm beyond the iron layer in the forward direction, 700 cm both laterally and backwards.

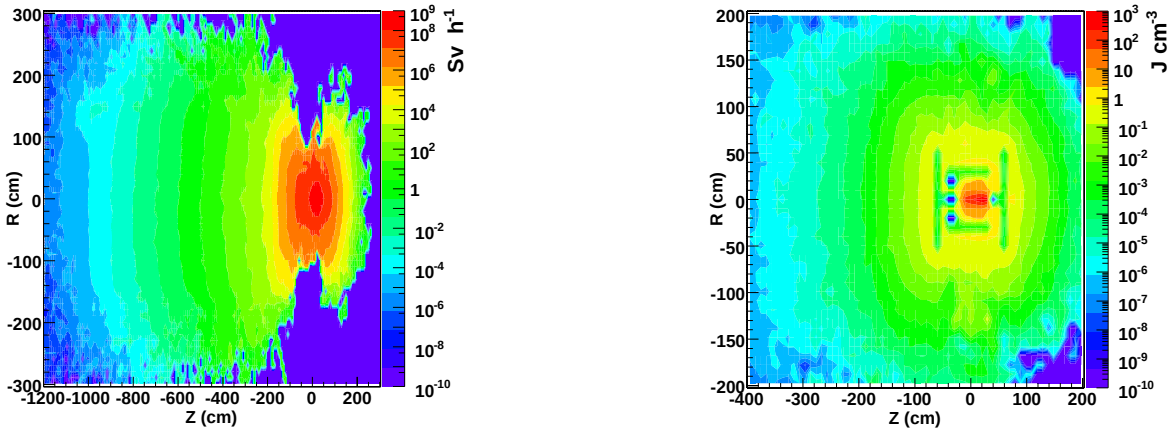

Figure 2: Calculated XZ map profiles in the middle plane of the shielding configuration for the neutron dose rate (left) and energy deposition by all transported particles (right)

The influence of other secondary particles produced in interactions with SS and concrete shields was investigated and it was found that their contributions to the total dose rate H*(10) is negligible. For instant, the ratio of H*(10) induced by photons to the total H*(10) is less than 2 % showing that the neutrons are dominant in the shielding estimates. Resulted energy deposition distribution presented in the right panel of Fig. 2 shows that the maximum of deposited energy is of the order of a few kJ cm^{-3} decreasing at the entrance in the SS zone values to around 1 J cm^{-3}.

3.1.2 Particle energy spectra

Fig. 3 shows the resulted particle energy distributions in the representative locations for SS shield and first concrete layer (concrete#1) in the forward direction. Statistical errors are included in

the graphs and are about 5 %.

These energy spectra show important differences. As expected, the photon fluxes are significantly lower than those of neutrons; the difference is by 15 % from the total flux for SS and by 25 % for concrete, while proton contributions are negligible (0.01% for both cases). Photons might be created inside the shielding through the cascade following high energy neutron interactions inside the shields. Most of the photons are created via de-excitation of residual nuclei after neutron inelastic scattering or through the capture of the thermal neutrons as prompt gammas. The photon energy spectrum range from about 0.01 to about 10 MeV. Besides the continuum Compton scattering of gamma-rays on the materials in the shielding, many discrete photon peaks of various intensities are seen in the graphs. These gamma lines are determined by the isotopic composition of the shielding materials. For instance, in the concrete the most distinct peaks are the 2.225 MeV gamma-ray from neutron capture on hydrogen, gamma emission following neutron capture in ^{28}Si (4.935 MeV) and the de-excitation of ^{16}O* (6.13 MeV). The presence of 0.511MeV gamma-rays is expected whenever photons are produced with energies above the pair production threshold. The conversion factors of the photons that are about two orders of magnitude smaller than those for neutrons explain the higher photon flux proportions comparatively with that of their associated dose rates (see discussion above).

The shape of the proton energy spectrum is similar to that of the high-energy neutrons, the major part having energy higher than 10 MeV. Protons are emitted preferably in the forward direction through the reactions between the high-energy neutrons and the various nuclei in the shielding.

The neutron energy spectra depicted in Fig. 3 are typical for high energy proton beam shielded by iron and concrete (see also [24]). Even though the fraction of neutrons carrying high energy (E > 20 MeV) coming directly from the spallation process is small (0.72 % for SS and 0.94 % for concrete#1) due to their large attenuation lengths these neutrons have an important contribution to the radiation field and the dose rates in the shielding. Deeply penetrating high energy neutrons are strongly peaked in the forward direction. The neutrons created in subsequent evaporation stage and emitted almost isotropically have a moderate impact on the shielding concern as they have lower energies and therefore can be attenuated in the most shielding material.

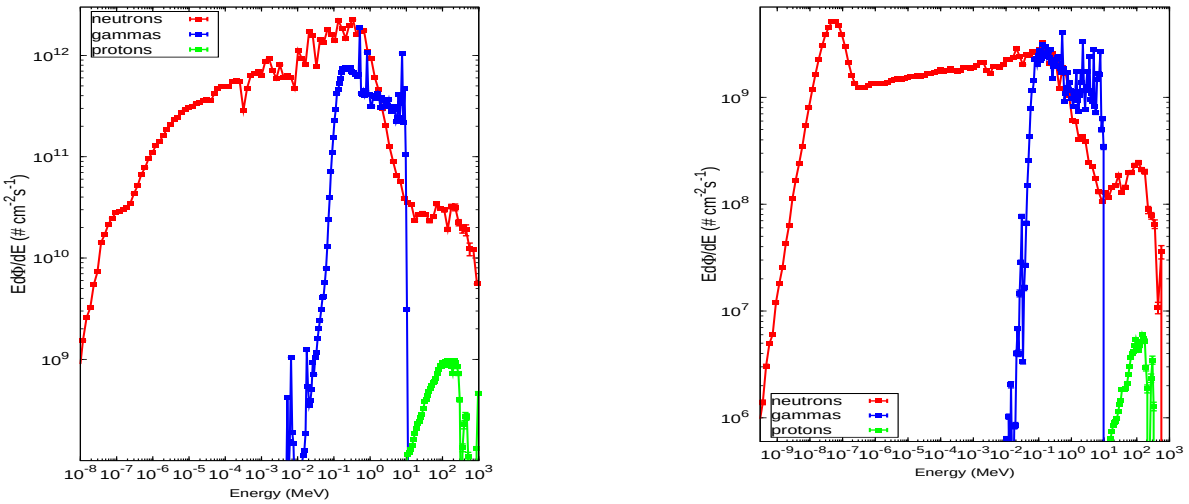

Figure 3: Energy distributions of neutrons, photons and protons obtained from simulations in the forward direction: (left) in the stainless steel layer and (right) in first concrete layer. Note the difference in scale of the Y axis for both figures.

At SS entrance the neutron flux is about 1.24*10^{13} cm^{-2} s^{-1}. Most of these neutrons come from the convertor target. This spectrum is modified due to the inelastic scattering and 24 keV resonance in iron. The major component of the spectrum is shifted to lower energy having a broad maximum

around a few hundreds of keV.

At entrance in the concrete#1 the neutron flux is in the order of $2.7*10^{10}$ cm^{-2} s^{-1}. A thermal peak followed by a close to 1/E distribution in the intermediate energy range characterizes the shape of this spectrum. The high-energy peak distributed around 100 MeV is particularly present in the forward direction. It consists mainly from the spallation neutrons that are transported through the iron shield without being significantly moderated. On the perpendicular direction as well with the increasing of the concrete depths this peak is considerably reduced.

The low energy neutron distributions at various depths of the shield used in activation calculations are presented in Fig. 4. The statistical errors included in the graphs are better than 5 %. Beyond two meters of concrete the variation in shape of the energy spectra shows differences from the entrance location. One observes the maximum around a few MeV as well as the deeper slope in the epithermal range. The identified peak comes from the neutron evaporation following neutron induced spallation reactions mainly on elements like oxygen and silicon. The sharp line laying at 2.35 MeV on the top of the evaporation peak corresponds to the ^{16}O minimum of the elastic scattering cross section. In the SS the low energy flux contribution (E < hundreds of keV) is appreciable reflecting the importance of the inelastic collisions of the high energy neutrons to produce neutrons in this energy range. This build-up effect results in a slower attenuation than that of the high energy component. At the interface with the concrete, this dominated contribution drops drastically showing the effectiveness of the concrete shielding performance due to elastic scattering effect of the hydrogen and further absorption of the low energy neutrons.

From the energy distributions in the concrete two main features are distinguished: i) below two meters of concrete these spectra reach the equilibrium and ii) the angle dependence of the energy spectra is increasingly pronounced with the depth in the concrete. For the first, it is seen from Fig. 4 that only amplitudes change with depth in the concrete but not the shape of the spectra and therefore the effective dose can be described using a single exponential formulation beyond this depth. The second feature is explained by the fact that the neutrons originate from various phases of the spallation process as was discussed earlier in this manuscript.

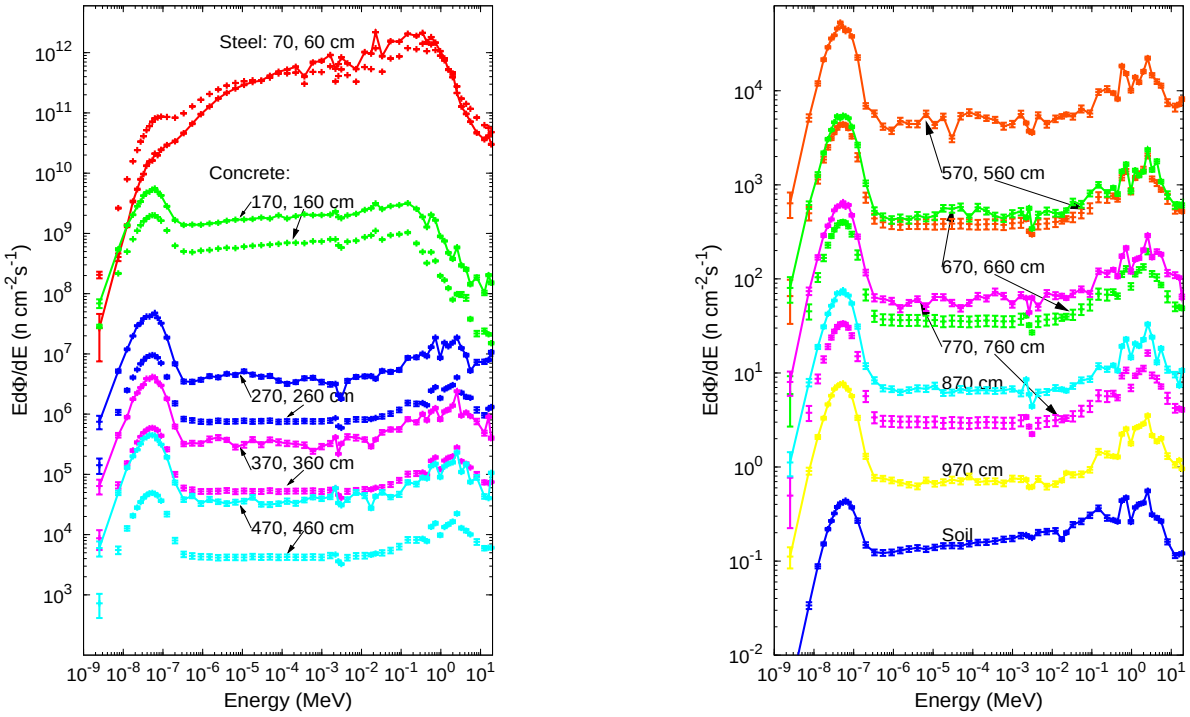

Figure 4: Low energy neutron flux energy distributions obtained in the representative locations. Lines: forward direction, points: lateral direction. Also see the legends for various shielding materials.

3.2 Induced radioactivity in the shielding

3.2.1 Activation inventory.

The results from activation runs are presented selectively for forward direction, SS and concrete#1 in Fig.5.

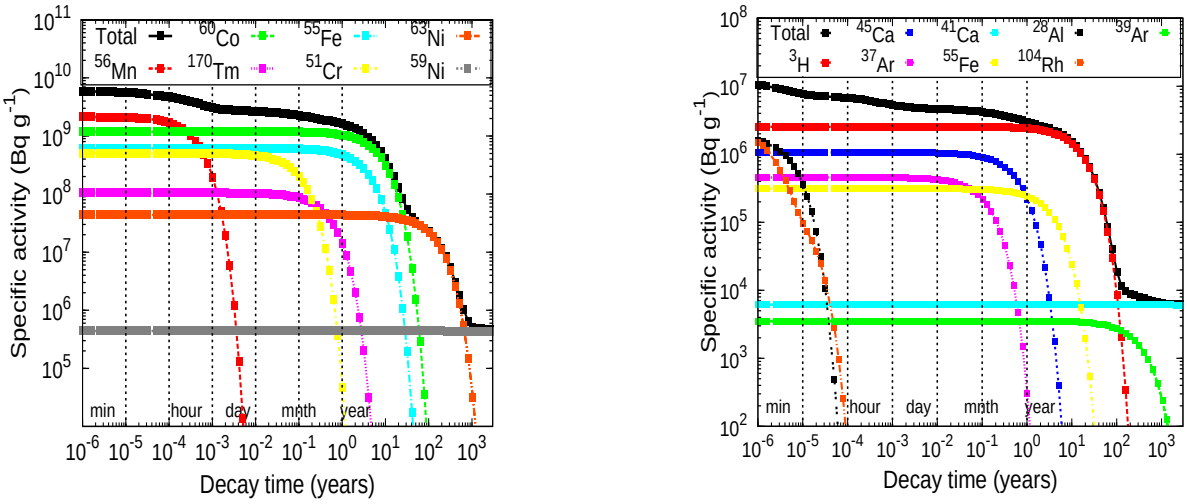

Figure 5: Sspecific activity in the forward locations: (left) dominant radioactive nuclides for stainless steel and (right) dominant radioactive contributions for the first concrete layer.

From the codes benchmarking it was found that DCHAIN-SP total specific activity results are by ~10 % higher than the CINDER'90 values with the largest isotope difference of a factor 1.6 standing for ^{170}Tm in SS and 2.5 for ^{137}Ar in case of concrete#1. Contribution of the high energy interactions upon the activation of the two selected items leads to an increased effect in the total specific activity of 25 % for SS over a cooling period of 1 year due mainly to ^{55}Fe and respectively 12 % in concrete#1 as consequence of the higher ^{3}H activity.

As seen from Fig. 5 during the first day after the end of operation, the main contributor to the activity is ^{56}Mn, while later, up to 10 years, ^{60}Co becomes dominant. After a decay time of 100 years the principal radionuclide is ^{63}Ni, and finally at very long time scales (1000 years) the most important radionuclide is ^{59}Ni. Note that after 40 years of operation, the SS becomes highly radioactive ($6*10^{9}$ Bq g^{-1} at the shutdown) and that even though at 1000 years after the shut-down the dominant isotope ^{59}Ni has a large L_i value due to the remaining high specific activity. For this reason, the derived CI will be likely greater than one. The specific activity of the concrete#1 is dominated by ^{3}H for a number of decades after cooling. On the other hand, within an interval of almost one month after the shutdown the percentage of the ^{3}H amount is little over the contributions of ^{45}Ca, ^{56}Mn, ^{28}Al, ^{37}Ar and ^{55}Fe. The relative contribution of ^{3}H becomes dominant over a large decay interval to almost 100 years. After 100 years of cooling the dominant isotope is ^{41}Ca. As for the SS the concret#1 becomes highly radioactive ($2*10^{7}$ Bq g^{-1} at the shutdown) and might be disposed of as radioactive wastes only. A rough examination of the obtained results draws to the conclusion that even at 1000 years the CI value might be greater than one (L_i for ^{41}Ca is $1.4*10^{3}$ Bq g^{-1}). The dependence in depth of the total specific activity is largely determined by the neutron flux spectra given in Fig. 4. Over a cooling interval of one century, these specific activity distributions are characterized by nearly time independent scaling factor. At longer times, the difference occurs due mainly to ^{39}Ar produced by the fast neutrons that characterized concrete strata beyond two meters.

3.2.2 Specific activity spatial distribution.

To visualize spatial distribution of the total induced specific activity through over entire shielding the derived maps are depicted in Fig.6 for the middle plane of the configuration. These graphs give information about activated shielding zones that control the quantities of the wastes to be disposed of as well as the physical distribution of the radionuclides presented in the materials.

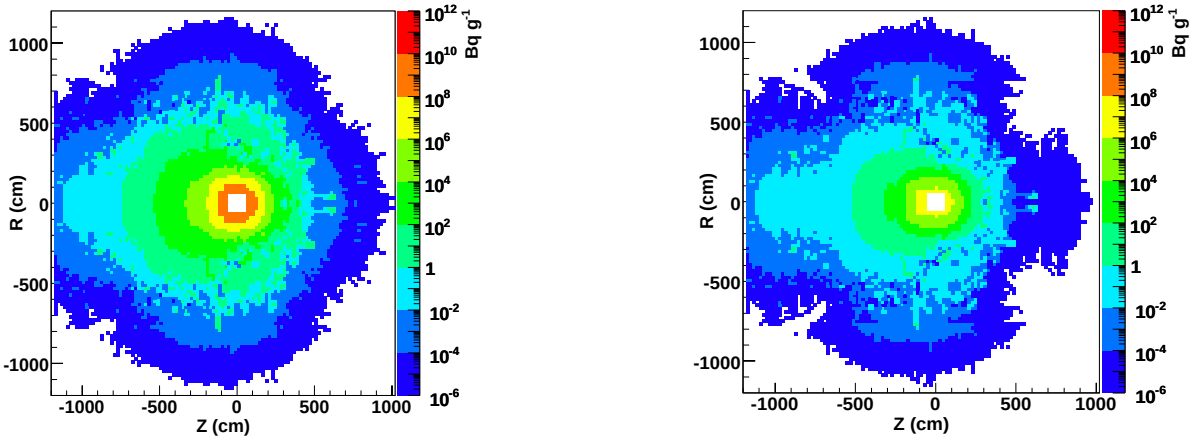

Figure 6: Derived maps of the total specific activity in the middle plane of the shielding configuration: (left) at 100 days decay time and (right) at 100 years decay time after the shutdown.

3.3 Waste categories.

The CI derived for the representative locations are shown in Fig. 7.

These results corroborate the preliminary conclusions about the SS and the concrete#1 layers; it is clear that the materials from these zones have to be disposed of in a final repository. It is also obvious that the concrete shielding has a potential for clearance beyond ~560 cm laterally even immediately after the shutdown time of the facility, while for the forward direction one year waiting time period is needed to declassify entire amount of concrete placed beyond ~670 cm.

The summary of activity and masses resulted from the activity calculations classified according with CI concept is shown in Fig 8. Even though the concrete shielding amount is very large (~10528 tons) comparatively with the corresponding SS quantity (~204 tons) the total activity inside the shielding is fully dominated by the SS component.

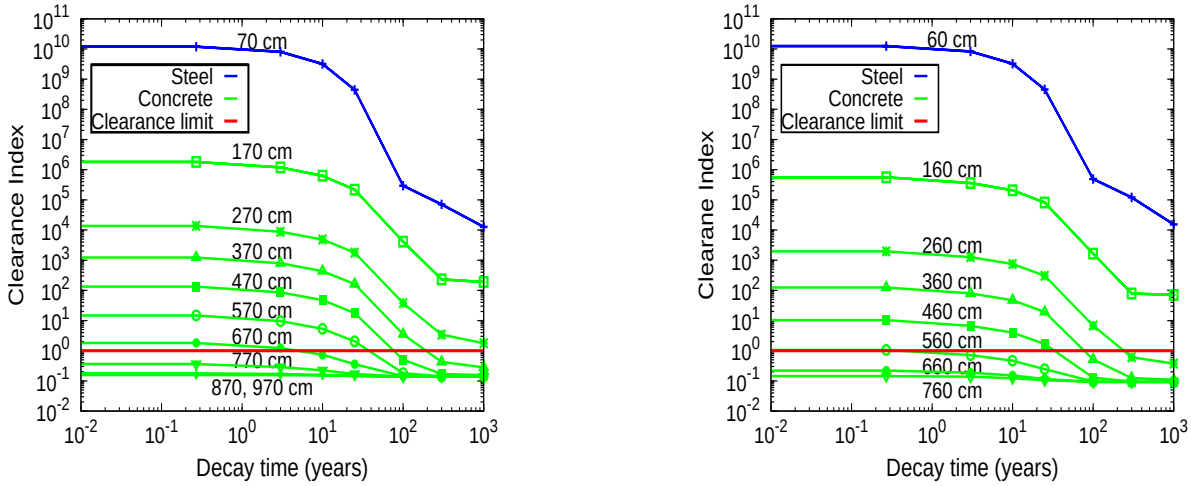

Figure 7: Derived clearance indexes in the representative locations: (left) for forward direction, and (right) for perpendicular direction.

As expected, the entire amount of the SS wastes from the shielding has to be disposed of as LL-ILW. Both approximations accounted lead to the same conclusion (only level of the activation is different). In case of the concrete shielding, precision of the method have important consequences not only on the magnitude of the radioactivity associated but also upon waste classification.

In the FM approach it was found that from the entire amount of the concrete wastes the quantity to be disposed of as LL-ILW represents almost 0.7 % over a long decay time period spanning up to 100 years. Further slightly decreasing of this percentage at ~0.6 % occurs at 1000 years of decay. In contrast, the amount of concrete to be disposed of as LL-ILW derived using TL approach is about 6.2 % from the total concrete mass along the entire time interval.

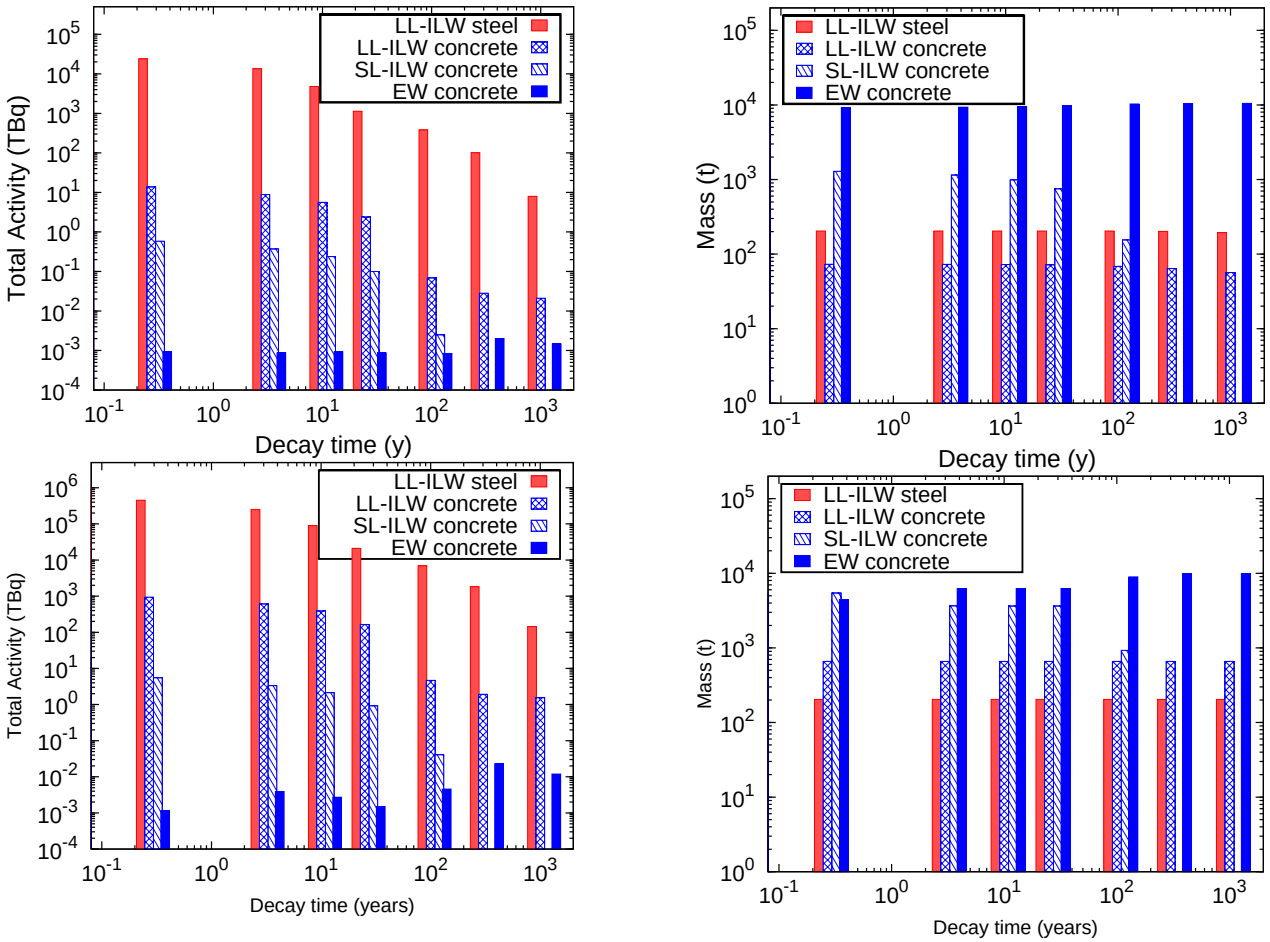

Figure 8: Waste categories of materials present in the shielding: activities (left) and masses (right). Fine Mesh (FM) tally approximation is shown at the top and the Thick Layer (TL) approach is shown at the bottom

Completing the above conclusion the obtained results show that large amounts of concrete might be classified as EW after the shutdown time of the facility: 80 % of the total concrete mass (FM approach) and respectively 42 % in case of the TL approach. The ratio of the EW percentages between FM and TL approaches reduces from a factor 2 (decay times until 100 days) through 1.5 (0.27 to 25 years) to almost 1 over 100 years. The remaining waste amounts defined as SL-ILW to be sent to an interim storage facility waiting for decaying might be further classified as EW.

The obtained differences in the above two approaches can be better understood from the specific activity profiles shown in the left side of Fig. 9. In this figure the histogram defines the levels chosen to model conservatively the activation in the thick layers of the shield, while the line stands for the detailed approximation. For both cases the derivation was done using representative specific

activity values indicated in the graph by points. Finally the comparison of the two approaches in the right panel of Fig 9 clearly shows the quantitative impact of the precision used for the activation estimates. The difference of the total activities arising from the shielding structure is greater by one order of magnitude. It is clear from this example that the most accurate approach (FM in our case) should be used to classify the wastes.

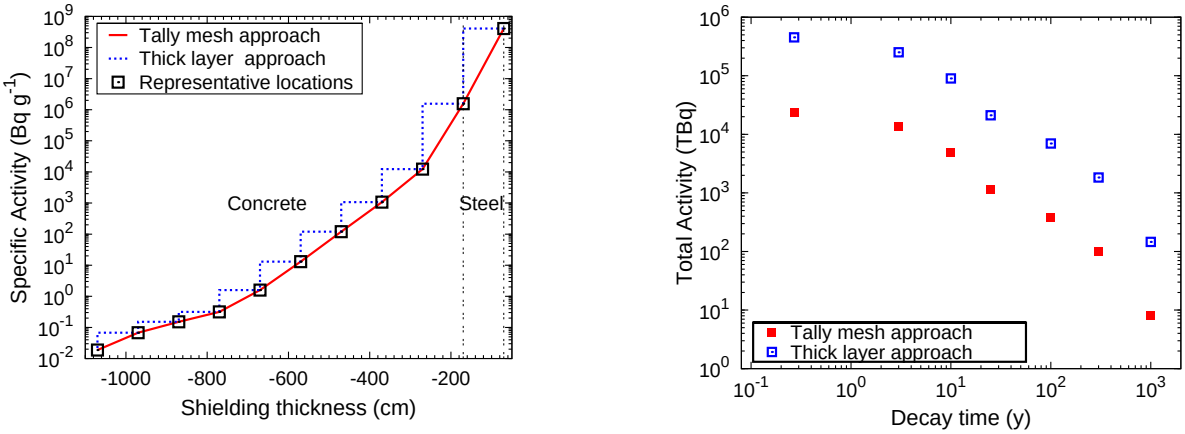

Figure 9: Comparison of the approaches: (left) specific activity profile in the forward direction at 10 years after the facility shut-down, (right) total activity associated to the shielding configuration.

An important point is worth to be mentioned. A significant contribution to the concrete activation is given by ^{3}H. It is known that tritium has a high mobility from metallic structures but scarce data are available regarding porous media. Follow up studies are necessary to clarify the amount of ^{3}H remaining bound in the water inside the concrete. In this stage it is desirable to have conservative estimates and therefore the waste classification accounted for entire tritium amount. Precise estimation of ^{3}H volatile gaseous diffused from the concrete shield under specific conditions (humidity, heat, etc.) is also necessary because it will act like a poison leading to contamination and representing therefore a supplementary risk hazard.

3.4 Source term for contaminant transport

The results for the ten most important isotopes from the point of view of the environmental risk assessment [26] are shown in Table 1.

Table 1: Specific activity [Bq cm^{-3}] in first 100 cm of soil/ground water surrounding the concrete wall after 40 years of continuous irradiation

Isotope	$T_{1/2}$	Soil	Groundwater
^{3}H	12.3 y	**1.62*10^{-4}**	**1.36*10^{-4}**
^{22}Na	2.60 y	**1.11*10^{-9}**	**8.43*10^{-8}**
^{24}Na	14.96 h	1.58*10^{-5}	6.60*10^{-7}
^{32}P	14.26 d	3.96*10^{-7}	4.92*10^{-7}
^{35}S	87.32 d	1.50*10^{-19}	2.62*10^{-7}
^{45}Ca	162.6 d	7.27*10^{-5}	7.25*10^{-8}
^{46}Sc	83.79 d	8.69*10^{-5}	3.56*10^{-21}
^{54}Mn	312.3 d	2.19*10^{-5}	2.81*10^{-11}
^{55}Fe	2.73 y	3.68*10^{-4}	6.75*10^{-10}
^{65}Zn	244.3 d	1.12*10^{-6}	1.69*10^{-10}

The standard deviation for the flux determination in the soil/groundwater beyond the concrete shield (see Fig. 4) was less than 5 %. Most of these radionuclides are produced by spallation. Fig. 10 complements the estimates presented in this table showing the radioactive dependence with decay time.

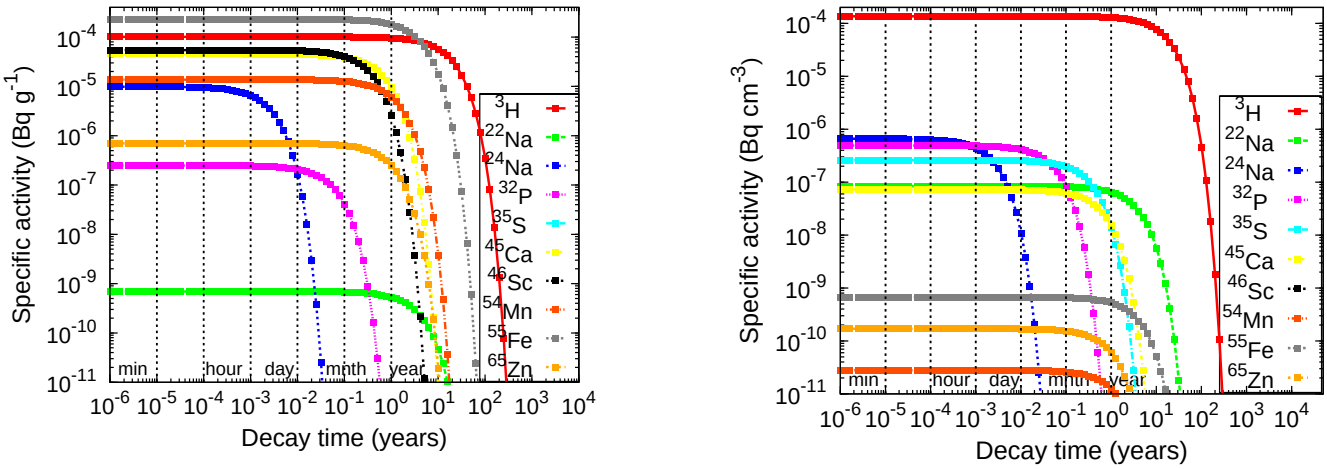

Figure 10: Specific activity of relevant radioisotopes in: (left) soil and (right) groundwater after 40 years of continuous irradiation and as a function of cooling time

The source term presented in the Table 1 was submitted to other group of specialists inside the project for a subsequent detailed environmental assessment study. Anyway, a rough examination of the obtained results shows that with a concrete shield of optimized thickness the present shielding design might be adequate from the point of view of the environmental impact.

From all radionuclides created in the soil ^{3}H and ^{22}Na can represent a hazard. They are in a soluble chemical form and have long half-lives. After 40 years of continuous operation in the 100 cm layer of soil surrounding the concrete shielding (Volume=1.1092*10^{9} cm^{3}) average estimates of 1.797*10^{5} Bq of ^{3}H and 1.231 Bq of ^{22}Na were found. If one compare these values with the derived generic clearance levels for liquid releases provided in [27] for ^{3}H of 10^{12} Bq y^{-1} (main exposure pathways: river – ingestion) and for ^{22}Na of 10^{5} Bq a^{-1} (main exposure pathways: sewage – external) it results clearly that the level of the soil activation is much lower than the annual release constrains. Similar conclusion is drawn analysing the groundwater results. It should be noted that the clearance levels mentioned above were derived to assure the compliance with an annual dose to the critical group of 10 μSv y^{-1}. One can conclude through this rough analysis that the transport of the radioactive species into the ground might not represent a hazard for the population.

Nevertheless a real evaluation of the environmental impact has to be done after the site of the facility will be chosen. Results of a hydro-geological study of the construction site and site specific data will provide a realistic evaluation of the exposure pathways as well as an accurate estimation of the fraction of the ground water that might reach the public water supplies.

3.5 Air activation

The radionuclide productions in the air shielding gap were firstly determined from Eq.2.3 using the data given in Fig. 11. Because of the relevant interaction cross sections data available in the literature, the calculation accounted only for the nuclides produced by the neutrons. In the air region, the neutron flux is about 1.32*10^{13} cm^{-2} s^{-1}, what is comparable to the value found at the entrance in SS.

Even though the fluxes of particle estimated by PHITS code reproduce those obtained by

MCNPX in the air region, as reported in Table 2 the resulted radionuclide yields depend of the nuclear data estimates. The high difference found for ^{11}C comes from the fact that PHITS approach result represents the cumulative production from ^{14}N irradiated by protons together with that arising from ^{16}O in the reactions with both neutrons and protons.

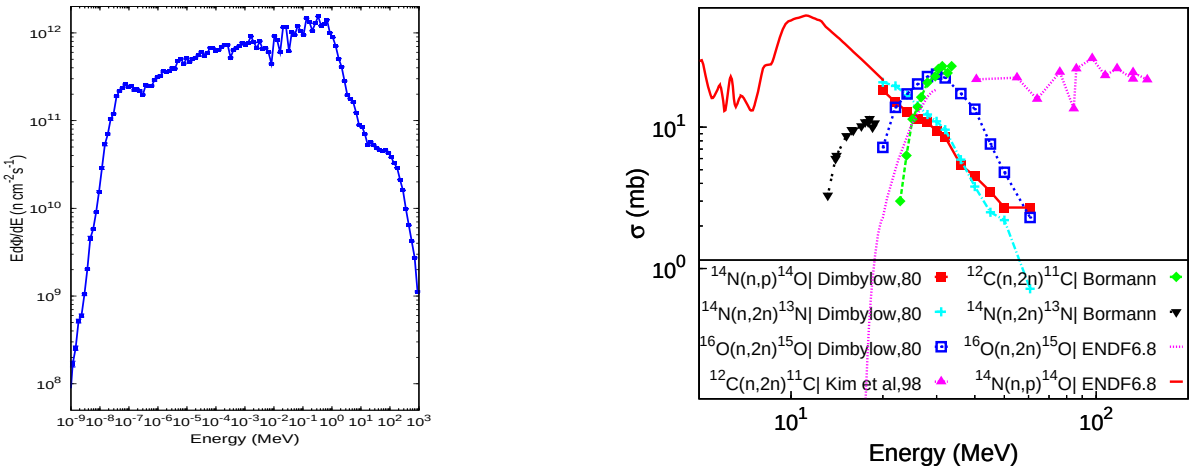

Figure 11: Input data used for estimating the radionuclide yields in the air region: (left) neutron spectrum resulted from MCNPX simulation and (right) measured and evaluated excitation functions of the radionuclide productions in the air (see the legend)

Table 2: Radionuclide production rates [# cm^{-3} proton^{-1}] obtained in the air region and derived through the two methods employed including their ratio.

Isotope	PHITS	Cross sections	PHITS/ Cross sections
^{14}C	$1.46*10^{-11}$	$3.93*10^{-12}$	3.7
^{11}C	$1.09*10^{-11}$	$2.70*10^{-15}$	4037
^{15}O	$7.36*10^{-12}$	$1.58*10^{-12}$	4.7
^{13}N	$1.68*10^{-11}$	$3.61*10^{-12}$	4.7

In Fig. 12 one can see the total specific activity and dominant contributions in the air region as a function of time over irradiation period of 125 days followed by a long decay time to 1000 years.

The short-lived positron emitters such as $^{14,15}O$, ^{13}N that are produced in oxygen and nitrogen by spallation reactions as well as ^{41}Ar created by the thermal neutron capture in the natural argon induce in the air a total activation of $6.25*10^{5}$ Bq cm^{-3} at the operation shut-down time. While for longer decay times ^{7}Be and ^{3}H and further ^{14}C are dominants.

For a realistic operation scenario (12 irradiation days) the activation level is roughly the same for a time period up to one day from the beam switched off due to the saturation of the short living nuclides for the conservative case. At longer cooling times the irradiation period becomes more important and the ratio between results reflect the irradiation time ratio between the two scenarios.

At the shutdown time moment, the difference in the total activation resulted from the two approaches (see Table 3) is due mainly to ^{13}N yield. As can be seen ^{11}C contribution has a negligible impact on the total activity while the difference in ^{14}C yields is not induced upon the radioactive product.

Relevant differences are observed in the relative contributions of the major components in the

resulted total activity. At shutdown time the leading nuclide in the radioactive inventory derived from the CS approach is ^{41}Ar reflecting the importance of the neutron low energy flux in this case.

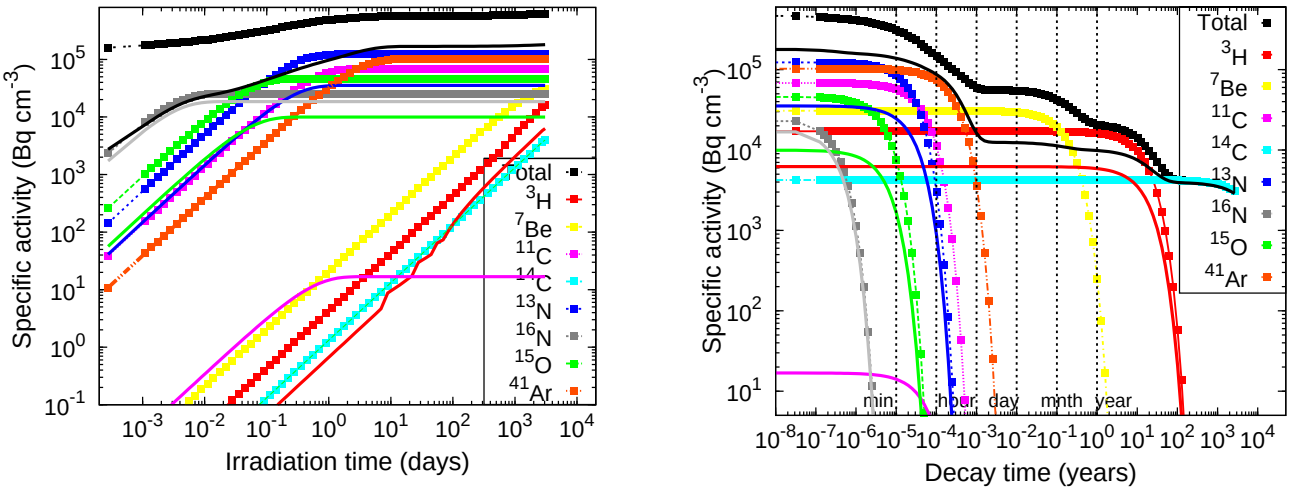

Figure 12: Specific activity of relevant radioisotopes in the air region vs. time: (left) under irradiation and (right) after shut-down. In the figure both results calculated with PHITS (symbols) and using the available cross sections data (lines) are given with the same color for comparison.

For the PHITS approach the total activity is dominated by the residuals produced in high energy reactions, while the activation product (n,γ)^{41}Ar represents only small contribution to the total. At longer decay times the difference between results is increased due to the contribution of spallation products as ^{7}Be and ^{3}H not included in the CS approach.

Table 3: Estimates of the produced radioactivity inside the air gap after 125 days of continuous irradiation. Dominant radioisotopes and their contributions to the total activity derived through the two methods employed are given.

Isotope	**PHITS**		**Cross sections**		**PHITS/ Cross sections**
	[Bq]	%	[Bq]	%	
^{13}N	9.160*10^{10}	19.7	2.6370*10^{10}	19.6	3.5
^{41}Ar	7.637*10^{10}	16.4	7.6365*10^{10}	56.7	1.0
^{11}C	5.080*10^{10}	10.9	1.2546*10^{7}	<0.1	4049
^{12}B	3.854*10^{10}	8.3			
^{15}O	3.430*10^{10}	7.4	7.4299*10^{9}	5.5	4.6
^{12}N	2.471*10^{10}	5.3			
^{7}Be	2.295*10^{10}	4.9			
^{16}N	1.879*10^{10}	4.0	1.3794*10^{10}	10.2	1.4
^{14}O	1.473*10^{10}	3.2			
^{3}H	1.273*10^{10}	2.7	4.6227*10^{9}	3.4	2.8
^{14}C	3.157*10^{9}	0.7	2.9532*10^{9}	2.2	1.1
^{37}Ar	1.887*10^{9}	0.4	1.7171*10^{9}	1.3	1.1
Total	**4.653*10^{11}**		**1.3460*10^{11}**		**3.5**

One can conclude from this analysis that for radiological safety in the shielding design the accurate determination of the activation cross sections of oxygen and nitrogen is an important requirement. The obtained estimates may be used to investigate scenarios of evacuation of the activated air. The results show that the air activation in the shielding gap is very high.

4. Conclusions.

A calculation procedure was developed in the scope of the radiological characterization of the shielding of multi-MW EURISOL target and further classification of the wastes arising during expected 40 years of the facility operation. Using the same approach the radionuclide production in the soil/groundwater surrounding the shielding was also derived. Activation of the air in the shielding gap, separating target assembly and shielding structures was further estimated by two approaches.

In agreement with the objective of this paper the main results of the performed study were: i) optimization of the size of the shielding for a composite structure of one metre of AISI304 stainless steel followed by a massive ordinary concrete block; ii) identification of the key radio-nuclides produced as well as the main pathways that lead to their production; ii) derivation of the activation spatial distribution over whole shielding configuration using two levels of approximation; iii) classification of the radioactive wastes based on the clearance index concept and comparison of the results derived using the two degrees of detail; iv) determination of the source term for contaminant transport in soil and groundwater; v) estimation of the air activation inside shielding gap.

Additionally, the main findings of the complex analysis performed are subsequently summarised.

The precision in activity estimates may have important consequences upon derived level of radioactivity of materials and their classifications as wastes. For instance, in the study it was found that more than one order of magnitude difference in the estimates of activation of the stainless steel shield.

Scaling of the induced radioactivity throughout the complete shielding configuration is a reasonable approximation and is the easiest way to obtain the first quick estimation. More accurate results of the radioactivity induced in the shielding requires a detailed study possible using Monte Carlo codes and able to give online results for very large models.

A sensitivity of activation analysis might be useful to decide the choice of the appropriate shielding material to be used in terms of safety and radioprotection, contributing to the reduction of the hazard risk and consequently of the cost estimates.

One can concluded also through the analysis of the contaminant source term values that the proposed shielding design might be adequate from the point of view of the environmental impact.

And finally the calculations have shown that the accurate determination of the activation cross sections of oxygen and nitrogen over large energy domain and for various incident particles is an important requirement.

The calculation methods developed here as well as the conclusions drawn from the present analysis will be used for the shielding of the MAFF-like target and direct targets concepts that yet have to be conceived [29].

Classification of wastes arising from the shielding of the multi-MW target has a strong impact on the decision and the strategy to be adopted for dismantling and final storage of the EURISOL facility. Accurate estimation of the activity inside the shielding is a very important issue having further consequences overall timescales and costs of the entire installation.

Acknowledgements

The authors thank to Dr. D.G. Cepraga for provision of the ANITA code Clearance Data File as well as for useful discussions on the IAEA clearance concept application.

We acknowledge the financial support of the EC under the FP6 "Research Infrastructure Action - Structuring the European Research Area "EURISOL DS Project; Contract No. 515768 RIDS; www.eurisol.org. The EC is not liable for any use that may be made of the information contained herein.

References

[1] EURISOL Design Study, http://www.eurisol.org

[2] M. Felcini, et al., Design of the EURISOL Multi-MW target assembly: Radiation and Safety issues, in *Proceedings of the SATIF-8 Workshop, Pohang Accelerator Laboratory, May, 2006*.

[3] A. Fassò, A. Ferrari, J. Ranft, and P.R. Sala, *FLUKA: a multi-particle transport code*, CERN-2005-10 (2005), INFN/TC_05/11, SLAC-R-773.

[4] IAEA, Classification of Radioactive Waste, A Safety Guide, IAEA Safety Series No.111-G-1.1, Vienna 1994

[5] IAEA, Clearance Levels for Radio-nuclides in Solid Materials: Application of the Exemption Principles, Interim Report for Comment, IAEA TECDOC-855, Vienna, 1996

[6] IAEA, Derivation of Activity Concentrations Values for Exclusion, Exemption and Clearance, Safety Reports Series No. 44, Report RS-G-1.7, STI/PUB/1213, IAEA, Vienna, 2005.

[7] A. Herera, Y. Kadi, 2006. EURISOL-DS Multi-MW target neutronic calculations for the baseline configuration of the Multi-MW target, CERN-AB-Note-2006-035 ATB, EURISOL-DS/TASK2/TN-05-0.

[8] MCNPX Monte Carlo N-Particle Transport Code System for Multiparticle and High Energy Applications; http://mcnpx.lanl.gov

[9] B. Rapp, J.C. David, V. Blideanu, D. Doré, D. Ridikas, N. Thiollière, *Benchmarking of the Modelling Tools for the EURISOL DS project,* Proceedings of International Workshop on Shielding Aspects of Accelerators, Targets and Irradiation Facilities(SATIF-8), Pohang, South Korea, 22/05/2006 - 24/05/2006

[10] A Manual for CINDER'90 Version C00D and Associated Codes and Data, LA-UR-00-Draft, April 2001.

[11] T. Kay, F. Maekawa, K. Kosako, et al, 2001. DCHAIN-SP 2001: High Energy Induced Radioactivity Calculation Code.

[12] R. A. Forrest, and J. Kopecky, The European Activation File: EAF cross section library. EASY documentation Series, UKAEA FUS 451, Culham Science Centre (2001)

[13] Association Française de Normalisation, AFNOR, http:/www.afnor.org

[14] Inventaire et Compositions Chimique des Matériaux du Réacteur ULYSSE de Saclay, DAPNIA/ SENAC/E/05-193/NT. (2005)

[15] B. Schlogl, R. Nabbi, R. Moormann, 2007. "Calculation of the Activity Inventory of Transportable Radionuclides in Soil and Groundwater for Large Neutron Sources", EURISOL DS/Task5/TN-07-01.

[16] International Commission on Radiological Protection,*'Limits for intakes of radionuclides by workers'*, ICRP publication 30, Parts 1-3 (1979-1981) and Supplements to Parts 1-3 (1979-1982), Pergamon Press, Oxford.

[17] D. G. Cepraga, G. Cambi, M. Frisoni, ANITA2000, NEA Data Bank Program NEA-1638, OECD Nuclear Energy Agency, (2000)

[18] D. G. Cepraga, private communication, 2007

[19] Annals of the ICRP Publication 72, International Commission on Radiological Protection 1993-1997, Age dependent Doses to Members of the Public from intake of radio nuclides: Part

5 Compilation of Ingestion and Inhalation Dose Coefficients, ICRP Publication 72, Elsevier Science, 1996
[20] National Nuclear Data Centre On-line Data Service, http://www.nndc.bnl.gov/
[21] Iwase, H., Niita K., Nakamura T., 2002. J. Nucl. Sci. Technol. 39(11), 1142
[22] S. Furihata, et al., 2001, The GEM Code -A simulation program for the evaporation and fission process of an excited nucleus, JAERI-Data Code 2001-015, JAERI, Tokaimura, Japan.
[23] S. Furihata and H. Nakashima, Analysis of activation yields by INC/GEM, JAERI-Conf 2001-006, 2001
[24] I. Koprivinkar, E. Schachinger, The biological shield of a high-intensity spallation source: a Monte Carlo design study, Nuclear Instruments and Methods in Physics Research A 487 (2002) 571
[26] Thomas R. H., Stevenson, G. R, 1988. Radiological safety aspects of proton accelerators. Technical Reports Series No. 283, Vienna, IAEA
[27] IAEA, 1998 Clearance of materials resulting from the use of radionuclides in medicine, industry and research, IAEA TECDOC-1000, Vienna, 1998
[28] A.H. Sullivan, 1992, A Guide to Radiation and Radioactivity Levels Near High Energy Particle Accelerators, Nuclear Technology Publishing Ashford, TN23 1JW England.
[29] Y. Kadi, J. Lettry, M. Lindroos, D. Ridikas, Th. Stora, L. Tecchio, "EURISOL High power targets", Nuclear Physics News, **Vol. 18** (2008) 19